PAPER • **OPEN ACCESS**

Synthesis, characterization and adsorption behaviors of Faujasite-type zeolites towards methylene blue

To cite this article: Yunhui Zhang *et al* 2019 *IOP Conf. Ser.: Mater. Sci. Eng.* **592** 012017

IOP Conf. Series: Materials Science and Engineering **592** (2019) 012017 doi:10.1088/1757-899X/592/1/012017

Synthesis, characterization and adsorption behaviors of Faujasite-type zeolites towards methylene blue

Yunhui Zhang, Zhongwei Wang, Zhenguang Zhang, Liuming Wu, Yingju Fan, Zhongxi Sun*

School of Chemistry and Chemical Engineering, University of Jinan, Jinan 250022, China

sunzx@ujn.edu.cn, +86-(0)531 8276 5426

Abstract. The conventional hydrothermal method was applied to synthesize two microporous Faujasite-type zeolite (FAU) with model substances (sodium silicate, sodium hydroxide and aluminium). The chemical formula of FAU-1 and FAU-2 were $0.99Na_2O{\cdot}Al_2O_3{\cdot}4.07SiO_2{\cdot}5.7H_2O$ and $1.03Na_2O{\cdot}Al_2O_3{\cdot}3.8SiO_2{\cdot}8H_2O$, respectively. The isoelectric points (IEP) were around 4.5, and the surface area were 244.50 m^2/g and 485.85 m^2/g. The adsorption kinetics, intra-particle diffusion and isotherms of methylene blue (MB) on two FAUs were reported from batch adsorption tests. The adsorption obeys pseudo-first-order model and reached equilibrium within 80 min. Intra-particle diffusion is the rate-determining step and the removal decreased with the increase of pH. The adsorption follows BET model, indicating multi-molecular layer adsorption. The adsorption capacity of FAU-2 towards MB is 147.19 mg/g, more than doubles that of FAU-1 (62.74 mg/g). Adsorption mechanism may include ion exchange, hydrogen bonding and hydrophobic interactions. This study may provide guidance for the hydrothermal synthesis of FAU and the universal theoretical basis for its practical application in MB contaminated wastewater treatment.

1. Introduction

Water pollution has become a public concern in recent decades with the rapid economic and industrial development. Dye pollutants have been discharged to the water body and other environmental media by various industries, such as textiles, dyeing and printing [1], leading to adverse effects on ecosystems and health risks to living organisms due to their toxicity [2]. Methylene blue (MB) is the most widely used organic dye and a typical pollutant used to simulate dye wastewater. Although it is not highly toxic [3], the exposure can do harm to eyes, respiratory, nervous and mental systems, and produce a burning sensation, increase sweating and cause methemoglobinemia [4].

The removal of MB has been investigated by many physico-chemical and biological treatments [2,3,5]. Adsorption has been proved to be a sustainable and effective approach to decontaminate dye effluents [1,4,6] due to its low cost, no secondary pollutants, simple design and high efficiency. Activated carbon has been a commonly used adsorbent for dye abatement. However, the high cost, the existence of organic impurity and difficult regeneration limit its application. Therefore, it is critical to find out an economical, eco-friendly and efficient adsorbent and explore its adsorption mechanisms. Zeolites, as a class of nanoporous aluminosilicates with a large surface, high reactivity, low cost, molecular sieve properties and high ion exchange capacity, have been applied for the removal of a broad range of pollutants [7–9]. Synthetic zeolites, with high purity and controllable surface areas and particle sizes, are ideal adsorbents and the study of their adsorption mechanisms has universal

meanings. Faujasite-type zeolite (FAU) is one of the most important zeolites and should be an ideal candidate for dye removing. It has been extensively used in catalysis [10], separations [11], ion exchange [12] and petroleum and petrochemical industry [13]. However, there is a dearth of literature on its adsorption performance towards organic dyes. Compared with natural zeolites, synthetic zeolites have higher purity, more homogeneous particle sizes and controllable surface areas, thus are more suitable for the study of adsorption mechanisms. Therefore, FAU was selected as a typical zeolite and synthesized by the conventional hydrothermal method for MB removal.

The objective of this study is to synthesize FAUs with model substances and discuss their adsorption mechanisms towards MB in order to provide the universal theoretical basis of the practical application of zeolites in cationic dyes decontamination. This study aims to 1) use model substances to synthesize two FAUs with different surface areas; 2) explore the detailed adsorption mechanisms towards MB; 3) discuss the effect of pH on the adsorption; 4) evaluate the effectiveness and feasibility of FAU in MB abatement. This study is expected to provide guidance for the hydrothermal synthesis of FAU and the theoretical basis of its practical application in MB contaminated wastewater treatment.

2. Materials and methods

2.1. Materials

$Na_2SiO_3 \cdot 9H_2O$, NaOH, aluminium powder, nitric acid, sodium hydroxide, sodium nitrate and methylene blue ($C_{16}H_{18}ClN_3S$) were purchased from three companies: Sinopharm chemical reagent company, Tianjin Shentai chemical reagent company and Tianjin Kaitong chemical reagent company. The concentration of methylene blue was measured by UV-vis spectrophotometer (Shimadzu, UV 2450) at the wavelength of 664 nm.

2.2. Synthesis of FAUs

$Na_2SiO_3 \cdot 9H_2O$ (a g) was dissolved in b mL of distilled water with stirring to produce Solution A. c g of NaOH granular was dissolved in distilled water with stirring, followed by the addition of d g of aluminium powder slowly and stir for 1 h to produce $NaAlO_2$ solution (Solution B). Subsequently, the filtered Solution B was added slowly into Solution A with continuous stirring in a pre-heated water bath at 30°C for 5 h. The produced white gel was transferred into an autoclave for aging at 30°C for 18 h and then at 90°C for 36 h for aging and crystallization, respectively. The obtained samples were washed with distilled water and ethanol and dried at 70°C for 12 h. The values of a, b, c and d for FAU-1 and FAU-2 are listed in Table 1.

Table 1. Experimental parameters for the synthesis of FAUs

	a	b	c	d
FAU-1	13.8	30	1.6	0.54
FAU-2	6.9	50	0.4	0.27

2.3. Characterization of synthetic FAUs

Characterization included X-ray diffraction (XRD), Fourier Transform Infrared Spectroscopy (FT-IR), zeta potential and BET analysis. A Bruker-AXS D8 ADVANCE X-ray diffractometer with a Cu target (Kα=1.5432 Å) was used to collect XRD powder patterns for the samples. XRD patterns were run at 40 kV and 30 mA with 2θ angles of 10° and 70° and the scanning speed was 0.02°/s. The FT-IR measurements (Vertex 70) were recorded at 4000–500 cm^{-1}. N_2 adsorption/desorption isotherms were obtained at 350°C with a Quantachrome NOVA 2000e surface and pore size analyzer by a static adsorption procedure. Zeolite samples (0.01 g) were added to the solution with the solid/liquid ratio of 0.4 g/L and the ionic strength of 1 mM $NaNO_3$ with pHs of 3-9.

2.4. Adsorption of methylene blue (MB)

Batch kinetic studies were carried out by adding 0.01 g of FAU into centrifuge tubes containing 25 mL 0.01 mM of MB solutions. After shaking for a certain time (10 min, 30 min, 50 min, 60 min, 70 min,

80 min, 120 min, 150 min and 180 min), the tubes were centrifuged for 5 min. The MB concentration of the supernatant was then measured. FAU (0.01 g) was added to 25 mL solutions containing different MB concentrations (0.01, 0.1, 0.3, 0.4, 0.8 and 1 mM) to obtain the adsorption isotherms. The shaking time was 3 h. The effect of solution pH was examined by adjusting the initial pH of the solutions from 3 to 9 using 0.1 M HCl or 0.1 M NaOH. The MB concentration was 0.01 mM and 0.01 g of FAU was used with a solid to liquid ratio of 0.4 g/L.

3. Results and discussion

3.1. X-ray diffraction (XRD) patterns

XRD patterns in Figure 1 confirmed the synthesis of two FAU zeolites (Faujasite-Na) by the comparison with those of JCPDS (Joint Committee on Powder Diffraction Standards). From Figure 1a, the strongest peaks appeared at 27.769° and the composition of FAU-1 is $0.99Na_2O{\cdot}Al_2O_3{\cdot}4.07SiO_2{\cdot}5.7H_2O$ with a Si/Al ratio of 2.0. The diameter was calculated as 111.5 nm. It was shown in Figure 1b that the strongest peak appeared at 23.6°. The composition of FAU-2 was $1.03Na_2O{\cdot}Al_2O_3{\cdot}3.8SiO_2{\cdot}8H_2O$ with a Si/Al ratio of 1.9 with a diameter of 111.5 nm.

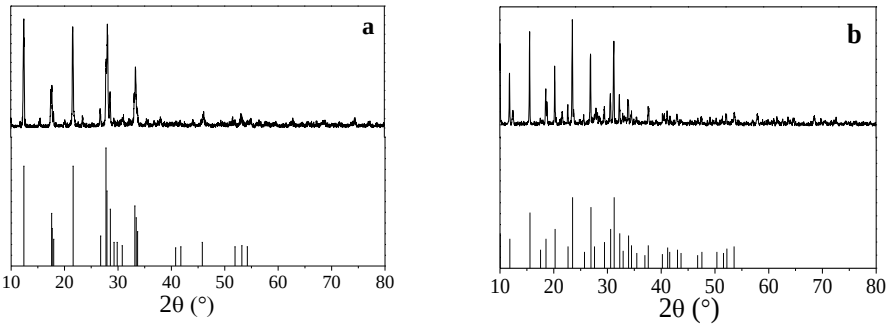

Figure 1. XRD patterns of synthetic FAU-1 (a) and FAU-2 (b) zeolites

3.2. Fourier Transform Infrared Spectroscopy (FT-IR)

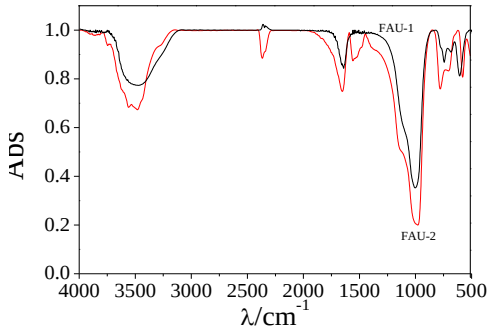

Figure 2. FTIR spectra of synthetic FAU-1 (a) and FAU-2 (b) zeolites

The FTIR spectra of two synthetic FAUs are similar as shown in Figure 2. Two FAUs are loaded with the different amounts of water indicated by different intensities of absorbance peaks, one at 3435 cm^{-1} due to O-H stretching vibrations and another at 1630 cm^{-1} due to O-H bending vibrations [14]. The peak at 3520±200 cm^{-1} was reported to be strongly interacting vicinal OH groups bound through the hydrogen bond [15]. Hunger et al. revealed that the difference in water absorption capacity of FAU zeolites depends on the different types of extra-framework cations and degrees of ion-exchange [16]. Therefore, the different amounts of water loaded in two FAUs may be explained by the different ion-exchange degree in consideration of the same cations (Na^+) in the framework of two FAUs. The water molecules were absorbed in FAU by the formation of cyclic hexamers which are linked with the framework of oxygen atoms by hydrogen bonding [17]. A band in the range of 1000 cm^{-1} was also

observed attributed to Si-O-Si asymmetric stretching vibration. Two peaks at 675 cm^{-1} and 737 cm^{-1} are caused by Si-O-Si symmetric stretching vibration, while the peak at 455 cm^{-1} is due to O-Si-O bending vibration. In addition, the peak in 2350 cm^{-1} is attributed to O=C=O asymmetric vibration absorption, indicating the absorption of CO_2.

3.3. BET measurement

The N_2 adsorption isotherms and particle distribution of microporous FAUs are shown in Figure 3. The isotherms were identified as the II type isotherm, indicating hydrophilic materials [14]. FAUs have high affinity to water at low and moderate pressure. The surface areas of FAU-1 and FAU-2 are 244.50 and 485.85 m^2/g, respectively. The difference in surface area may come from the different Si/Al ratio and amounts of NaOH. Synthesis of FAU with different amounts of model substances need to be conducted to explore their effects on the change of surface area.

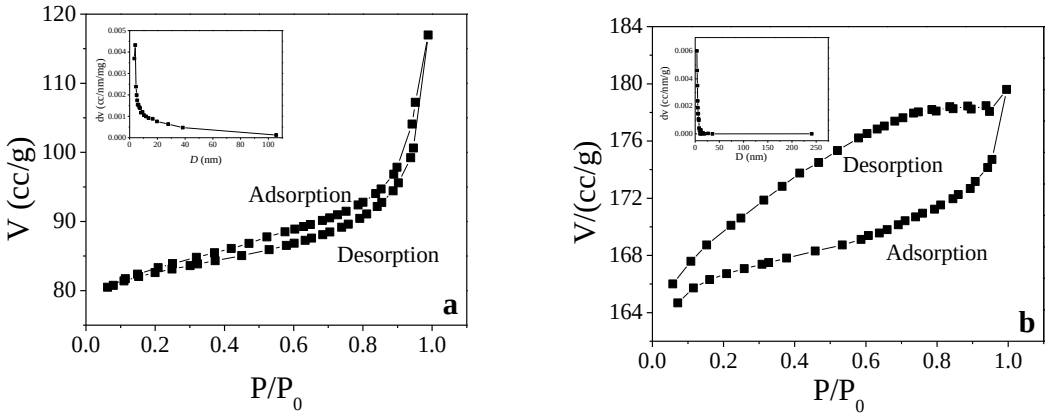

Figure 3. N_2 adsorption/desorption isotherms of synthetic FAU-1 (a) and FAU-2 (b) zeolites

3.4. Zeta potential

Zeta potential was measured based on the mobility of electrophoresis. Zeta potential of zeolites depends on the solution pH, ionic strength and the Al content of the framework [18]. Figure 4 shows the zeta potentials of FAUs as a function of pH at room temperature. The isoelectric points (IEP) of FAU-1 and FAU-2 were found to be around 4.5, meaning that their surface was mainly positively charged below a pH of 4.5 and became negative at higher pHs. The negative charges on the surface come from the isomorphous replacement of Al for Si in the lattice, i.e. permanent negative charge [19], as well as the adsorption of OH^- at different pHs.

3.5. Adsorption of methylene blue (MB)

3.5.1. Adsorption kinetics. Pseudo-first-order, pseudo-second-order models were used to fit the experimental data. Pseudo-first-order and pseudo-second-order models are most commonly used kinetic models. The coefficient of determination (R^2) and Akaike Information Criterion (AIC) were applied for model selection. A model with highest R^2 and lowest AIC values should be selected [7]. The fitting results are shown in Figure 5 and Table 2. Where q_e and q_t are the adsorbed amount of MB at equilibrium and at time t, respectively; C_e is the equilibrium MB concentration; k_1 and k_2 are the rate constants; $t_{1/2}$ is the time to uptake half of the amount adsorbed at equilibrium; D is the minimum MB removal asymptote; A is the maximum removal capacity. All kinetic models could describe the MB adsorption onto FAUs with R^2>0.85. However, pseudo-first-order models have the lowest AIC values for both FAUs. Therefore, the MB adsorption onto FAUs follows pseudo-first-order model. The MB adsorption reached equilibrium within 80 min for both FAUs.

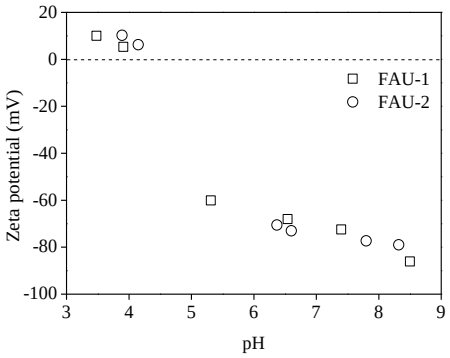

Figure 4. Zeta potential of two synthetic FAUs as a function of pH

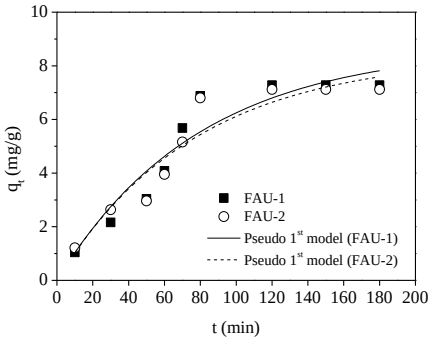

Figure 5. Adsorption kinetics of MB adsorption on two synthetic FAUs

3.5.2. Weber and Morris intra-particle diffusion model. Weber and Morris intra-particle diffusion model was applied to fit the plot of q_t against $t^{1/2}$ to describe the intra-particle diffusion process. The equation and piecewise linear fitting regression results are presented in Table 2 and Figure 6. Where k_i (mg/g/min$^{1/2}$) is the rate constant, and c is the intercept which suggests the thickness of the boundary layer. That is, the higher value of c indicates the greater effect of the boundary layer. The typical mass transfer process [20] of adsorbate from the solution to the binding sites within the adsorbent particles is shown in Figure 7, in the order of from the solution to the film, film diffusion, intra-particle diffusion and adsorption [7].

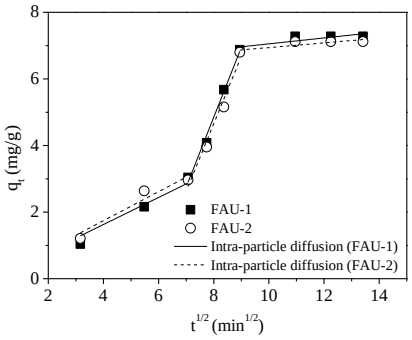

Figure 6. Intra-particle diffusion plot of MB adsorption on two synthetic FAUs

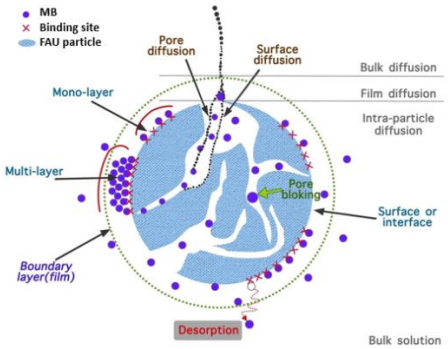

Figure 7. The mass transfer process of MB [20]

From Figure 6, there are three parts in the intra-particle diffusion plot. The first part indicates film diffusion at the outer surface where the MB molecules overcame the boundary layer resistance. The second part describes the intra-particle diffusion, including pore diffusion and surface diffusion, where the MB molecules have entered the pores of FAUs. Therefore, the intra-particle diffusion period was 50-80 min and the value of $k_{i,2}$ in this part was defined as the intra-particle rate constant, 0.51 and 0.46 mg/g/min$^{1/2}$ for FAU-1 and FAU-2, respectively. The last flat step is the equilibrium period. The intercept of the first portion is zero, i.e. the line covering the first part passed through the origin, indicating that intra-particle diffusion controlled the rate of MB adsorption on FAUs. That is, the resistance of the boundary layer is negligible, and film diffusion is very fast and can be ignored. FAU has a structure like a tiling of sodalite cages connected by double six-ring units. It is a typical microporous zeolite and the diameters of void space are 11.24 Å and 7.35 Å. Although the molecular diameter of MB is about 7.7 Å [21], the actual molecule dimension of MB is 16.32 Å × 5.64 Å × 5.41 Å in the solution due to the solvent effect [22]. This means that it is hard and time-consuming for MB molecules to enter the inner pores of FAU. Therefore, the adsorption of MB

may mainly occur on the outer surface and intra-particle diffusion process was non-negligible and controlled the adsorption rate.

3.5.3. Adsorption isotherms. The commonly used Langmuir, Freundlich and modified form of BET isotherm models were applied to fit the experimental data at different initial MB concentrations (0-0.8 mM) as shown in Figure 8 and Table 3. The high R^2 values (>0.95) indicated that the MB adsorption onto FAUs obeys the BET model, indicating the multi-molecular layer physical adsorption. The adsorption capacity of FAU-2 towards MB is 147.19 mg/g, more than doubles that of FAU-1 (62.74 mg/g) (Table 4). The adsorption of MB on zeolites and other adsorbents are compared as shown in Table 5. The adsorption capacities of MB molecules by surface area were calculated as 4.83×10^{17} and 5.70×10^{17} m^{-2} for FAU-1 and FAU-2, respectively. FAU-2 with a slightly lower Si/Al ratio has an 18% higher adsorption capacity excluding the effect of surface area. Therefore, the surface area is a main influencing factor and the Si/Al ratio may also have an effect on the adsorption capacity. The adsorbent with larger surface area provides more binding and adsorptive sites on the surface, leading to higher adsorption capacity. Although MB molecules are hard to enter the inner pores of FAU and a few adsorption sites in the inner surfaces of FAU are not available for MB molecules, the surface areas measured by BET from the N_2 adsorption isotherms in this study are mainly the external surface area, which reflects the MB adsorption on outer surface of FAU. In addition, the effect of Si/Al ratio may be attributed to the fact that more silica in the structure is replaced by aluminium on the surface of FAU-2, resulting in more negative charges and adsorption sites for MB.

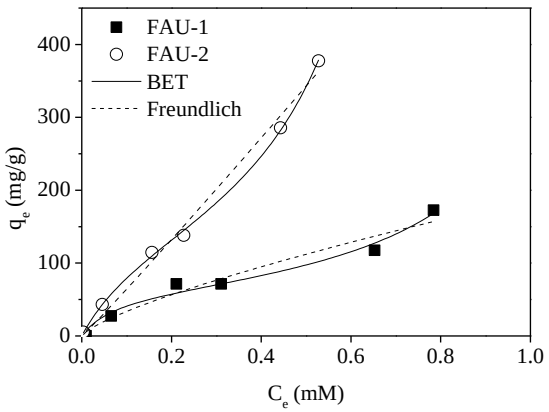

Figure 8. Adsorption isotherms of MB adsorption on two synthetic FAUs

Table 2. Kinetics model parameters for MB adsorption on two FAUs

Models	Equations	Parameters	FAU-1	FAU-2
Pseudo-first-order	$q_t = q_e(1 - e^{-k_1 t})$	q_e (mg/g)	8.72±1.21	8.39±1.08
		k_1 (min^{-1})	0.013±0.004	0.013±0.004
		AIC	4.30	3.19
		R^2	0.895	0.894
Pseudo-second-order	$q_t = \frac{q_e^2 k_2 t}{1 + q_e k_2 t}$ $t_{\frac{1}{2}} = \frac{1}{k_2 q_e}$	q_e (mg/g)	12.68±2.84	11.98±2.46
		k_2 (g/mg/min)	(7.42±4.90)×10^{-4}	(8.42±5.19)×10^{-4}
		AIC	5.43	4.30
		$t_{1/2}$ (min)	106	99.14
		R^2	0.882	0.883
Weber and Morris intra-particle diffusion	$q_t = k_i t^{1/2} + c$	Intra-particle diffusion period	50-80 min	
		$k_{i,2}$ (mg/g/$min^{1/2}$)	0.41±0.02	0.44±0.02
		C	0	0
		R^2	0.95	0.94

Table 3. BET isotherms model parameters for MB adsorption on two FAUs

Models	Equations	Parameters	Definition	FAU-1	FAU-2
Langmuir	$q_e = \frac{Q_0 b C_e}{1 + bC_e}$	Q_0 (mg/g)	Maximum adsorption capacity	428.06±271.61	
	$R_L = \frac{1}{1 + bC_0}$	b (L/mmol)	Rate of adsorption	0.73±0.67	
		R_L	Equilibrium parameter	0.99	
		R^2		0.93	Failed
Freundlich	$q_e = C_e^{\frac{1}{n}} K_F$	K_F (mg/g)	Adsorption capacity	188.46±17.91	705.16±59.63
		1/n	A measure of adsorption intensity or surface heterogeneity	1.33±0.24	0.96±0.09
		R^2		0.94	0.99
BET	$q_e = q_m \frac{K_S C_e}{(1 - K_L C_e)(1 - K_L C_e + K_S C_e)}$	q_m (mg/g)	Theoretical adsorption capacity	62.74±14.54	147.19±13.65
		K_L (L/mmol)	Equilibrium constants of first and second layer adsorption	0.82±0.10	1.22±0.05
		K_S (L/mmol)		13.63±11.69	7.87±1.82
		R^2		0.97	1.00

Table 4. Adsorption capacities of FAUs toward MB

Sample	Formula	Surface area	Si/Al	Adsorption capacity	
FAU-1	$0.99Na_2O{\cdot}Al_2O_3{\cdot}4.07SiO_2{\cdot}5.7H_2O$	244.50 m^2/g	2.0	62.74 mg/g	4.83×10^{17} m^{-2}
FAU-2	$1.03Na_2O{\cdot}Al_2O_3{\cdot}3.8SiO_2{\cdot}8H_2O$	485.85 m^2/g	1.9	147.19 mg/g	5.70×10^{17} m^{-2}

Table 5. Comparison of adsorption properties of MB with other adsorbents

Adsorbents	q_m (mg/g)	Kinetic model	Isotherm	Reference
Fly ash zeolite NaP1		Pseudo-2nd-order	Freundlich	[23]
Canola residues	11.25	Pseudo-2nd-order	Sips	[24]
Coconut husk-based activated carbon	434.78	Pseudo-2nd-order	Langmuir	[25]
Bentonite/zeolite-NaP composite	36.23	Pseudo-2nd-order	Langmuir	[26]
NaA zeolite	64.8	Pseudo-1st-order	Langmuir	[27]
Mordenite	0.026	Pseudo-2nd-order	Langmuir	[28]
Treated clinoptilolite	12.15	Pseudo-2nd-order	Langmuir	[2]
zeolite	22	Pseudo-2nd-order	Temkin	[29]
Graphene-carbon nanotube composite	65.79	Pseudo-2nd-order	Langmuir	[30]
FAU-1	62.74	Pseudo-1st-order	BET	This study
FAU-2	147.19	Pseudo-1st-order	BET	

3.5.4. Effect of pH. The solution pH is a critical influencing factor for surface property changes, such as surface charges of adsorbents and ionization of adsorbates as shown in Table 6. As shown in Figure 9, the MB adsorption on FAU-2 was higher than that on FAU-1 at all pHs. The MB adsorption on FAUs was the highest in acidic conditions, and the adsorption decreased with the increase of solution pH in the range of 3-9. This makes it possible to regenerate the saturated FAU at alkaline pHs, which is meaningful for the practical application of FAU in MB-contaminated water treatment. Generally, the adsorption characteristics at different pHs depend on the physiochemical properties of both adsorbent and adsorbate. The surface charge of the adsorbent changes at different pHs due to different IEPs. Different adsorbates have different pKa (acid dissociation constant) values, indicating a different degree of ionization. In addition, the functional groups of the adsorbents may also dissociate at different levels [31], especially for the surfactant-modified adsorbents. For example, Rida et al [29] revealed that the MB adsorption onto zeolite increased with the increasing pH in the range of 2-4.5, and decreased in the range of 4.5-12. This is likely due to the fact that the optimal pH is close to the pKa (3.8) of MB [3]. In comparison, Jin et al. reported that the MB adsorption on ZSM-5 increased with the increasing pH in the range of 4-5 and then remained steady due to the competition between

H^+ and cationic MB for adsorption sites and negatively charged surface under alkaline conditions, while this is different from the adsorption of anionic orange II, the adsorption decreased with the increase of pH due to the electrostatic repulsion between OH^- groups on the surface of ZSM-5 and anionic orange II. The adsorption of MB on surfactant modified ZSM-5 remained constant with the increase of pH [1].

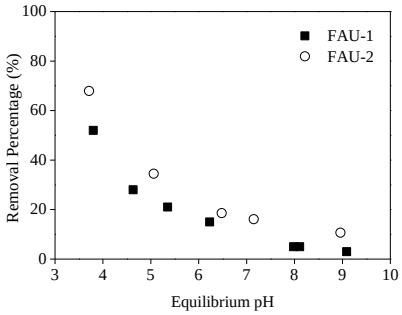

Figure 9. Effect of pH on MB adsorption

Table 6. Surface charges of FAU and MB

pH	FAU	Dominant MB species
pH<3.8	+	MBH^{2+}
pH=3.8	+	50% MBH^{2+}; 50% MB^+
3.8<pH<4.5	+	MB^+
pH>4.5	−	

The adsorption of MB decreased with the increase of solution pH in Figure 9, which is similar to that of Tsai et al. [32]. They synthesized a hydrophilic zeolite by hydrothermal method, and the decrease of adsorption toward MB with the increasing pH was explained by the increased surface area at lower pH caused by the interaction between H^+ and zeolite. In this study, the decrease of adsorption may be explained by the surface charges of FAU and MB species (Table 6). The divalent cation MBH^{2+} is the dominant form at pH<pKa of MB, while the main species is monovalent cation MB^+ at pH>pKa (Equation (2)) [33]. As shown in Equation (3) and Table 7, dimers, trimers or higher aggregates of MB ($(MB^+)_m$) may also form and could be adsorbed on zeolites [34–36]. In addition, it is well known that in a heterogeneous system, such as mineral suspensions, surface micells (dimer and trimer or aggregates) could form well below those in homogeneous system [37]. Positive charges are predominance on the surface of FAU at pH<IEP and the surface is negatively charged at pH>IEP. In the structure of FAU, some silica in the silica sheet is replaced by aluminium, and Na^+ acts to balance the produced net negative charges. As shown in Equation (4)-(8), when FAU is dissolved in the acidic solution, Na^+ in the structure begins to dissociate and H^+ at high concentrations neutralizes the negative charges. Afterward, H^+ is replaced by cationic MB species via ion exchange, resulting in a high adsorption. The complexation constants of MB with silanol groups on the surface of SiO_2 have been calculated in our previous study [38], and those between MB and aluminol groups need to be explored further in future. In comparison, silanol and aluminol groups could dissociate at neutral or alkaline conditions, making zeolites negatively charged. These negative charges on the surface of FAU may be neutralized by more Na^+ at higher pHs due to the addition of NaOH and monovalent MB^+ (Equation (9) and (10)), leading to the decreasing MB adsorption. Therefore, ion exchange may make a dominant contribution to the adsorption of MB onto FAU.

$MBH^{2+} \Leftrightarrow MB^+ + H^+$ pKa=3.8 Equation (2)

$m\ MB^+ \Leftrightarrow (MB^+)_m$ (m>1) Equation (3)

At acidic conditions:

$\equiv X_nONa \Leftrightarrow \equiv X_nO^- + Na^+$ (X=Si, Al; n=1, 2) Equation (4)

$\equiv X_nO^- + H^+ \Leftrightarrow \equiv X_nOH$ Equation (5)

$2 \equiv X_nOH + MBH^{2+} \Leftrightarrow (\equiv X_nO)_2MBH + 2\ H^+$ Equation (6)

$\equiv X_nOH + MBH^{2+} \Leftrightarrow \equiv X_nOMBH^{+} + H^{+}$ Equation (7)
$\equiv X_nOH + MB^{+} \Leftrightarrow \equiv X_nOMB + H^{+}$ Equation (8)
At alkaline conditions:
$\equiv X_nO^{-} + Na^{+} \Leftrightarrow \equiv X_nONa$ Equation (9)
$\equiv X_nOH + MB^{+} \Leftrightarrow \equiv X_nOMB + H^{+}$ Equation (10)

Table 7. Structures and wavelengths of different MB species

Species	Structure	Wavelength (nm)
MB^{+}	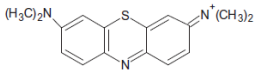	664 [42]
MBH^{2+}	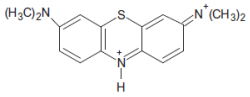 [48][a]	741 [42]; 763 [41]
$(MB^{+})_2$	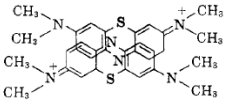 [48][a]	605 [41]; 697 [42]
$(MB^{+})_3$		580 [42]; 575 [41]

[a] one possible structure

3.5.5. Adsorption mechanisms. From the results of adsorption kinetics, isotherms and the effect of pH, the MB adsorption onto FAUs is the multi-molecular layer physical adsorption and the intra-particle diffusion is the rate-controlling step. It was reported that MB could be adsorbed on carbonaceous nanomaterials by non-covalent forces, such as hydrogen bonding, electrostatic interactions, π–π stacking, van der Waals forces and hydrophobic interactions [39]. The MB adsorption on FAUs in this study may be due to the combined approaches, i.e. ion exchange, hydrogen bonding and hydrophobic interactions. Firstly, as explained in Section 3.5.4, cationic MB species (MBH^{2+}, MB^{+})could be adsorbed on the surface of FAU via ion exchange, especially at acidic conditions when there are divalent ion MBH^{2+}. Secondly, hydrogen-bond interaction (O−H···N) may exist between the silanol and aluminol groups of FAUs and the electronegative nitrogen of MB [15,40]. After the adsorption sites on the surface are fully occupied, it may cause steric hindrance and residual MB species may interact with $\equiv X_nOH$ via hydrogen bonding. Hydrogen bonding may also explain the multi-molecular layer adsorption of MB onto FAU. Thirdly, the presence of hydrophobic siloxane (-Si-O-Si-) groups [15] may attract the organic part of MB, increasing the adsorption of MB onto FAU via hydrophobic interaction.

4. Conclusions

In this study, two Faujasite-type zeolites (FAU) with different surface areas were synthesized by the conventional hydrothermal method. Batch adsorption tests were also conducted to investigate the adsorption kinetics, intra-particle diffusion and isotherms of methylene blue (MB) on two FAUs. The following conclusions could be drawn: 1) The adsorption obeys the pseudo-first-order kinetic model; 2) Intra-particle diffusion controlled the rate of MB adsorption on FAUs; 3) The adsorption follows BET isotherms model; 4) Adsorption mechanism may be mainly ion exchange combined with hydrogen bonding and hydrophobic interactions.

Acknowledgments

This work was funded by National Natural Science Foundation of China (No. 51274104).

References

[1] Jin X, Jiang M qin, Shan X quan, Pei Z guo and Chen Z 2008 Adsorption of methylene blue and orange II onto unmodified and surfactant-modified zeolite *J. Colloid Interface Sci.* **328** 243–

7
[2] Bayat M, Javanbakht V and Esmaili J 2018 Synthesis of zeolite/nickel ferrite/sodium alginate bionanocomposite via a co-precipitation technique for efficient removal of water-soluble methylene blue dye *Int. J. Biol. Macromol.* **116** 607–19
[3] Barbosa L V, Marçal L, Nassar E J, Calefi P S, Vicente M A, Trujillano R, Rives V, Gil A, Korili S A, Ciuffi K J and De Faria E H 2015 Kaolinite-titanium oxide nanocomposites prepared via sol-gel as heterogeneous photocatalysts for dyes degradation *Catal. Today* **246** 133–42
[4] Rafatullah M, Sulaiman O, Hashim R and Ahmad A 2010 Adsorption of methylene blue on low-cost adsorbents: A review *J. Hazard. Mater.* **177** 70–80
[5] Ghaedi M, Hajjati S, Mahmudi Z, Tyagi I, Agarwal S, Maity A and Gupta V K 2015 Modeling of competitive ultrasonic assisted removal of the dyes - Methylene blue and Safranin-O using Fe3O4nanoparticles *Chem. Eng. J.* **268** 28–37
[6] Zhang P, Lo I, O'Connor D, Pehkonen S, Cheng H and Hou D 2017 High efficiency removal of methylene blue using SDS surface-modified ZnFe2O4 nanoparticles *J. Colloid Interface Sci.* **508** 39–48
[7] Zhang Y, Jin F, Shen Z, Lynch R and Al-Tabbaa A 2018 Kinetic and equilibrium modelling of MTBE (methyl tert-butyl ether) adsorption on ZSM-5 zeolite: Batch and column studies *J. Hazard. Mater.* **347** 461–9
[8] Xie J, Li C, Chi L and Wu D 2013 Chitosan modified zeolite as a versatile adsorbent for the removal of different pollutants from water *Fuel* **103** 480–5
[9] Ates A and Akgül G 2016 Modification of natural zeolite with NaOH for removal of manganese in drinking water *Powder Technol.* **287** 285–91
[10] Motazedi K, Mahinpey N and Karami D 2016 Preparation and Application of Faujasite-Type Y Zeolite-based Catalysts for Coal Pyrolysis using Sodium Silicate Solution and Colloidal Silica as Silicon Source *Chem. Eng. Commun.* **203** 300–17
[11] Mastropietro T F, Brunetti A, Zito P F, Poerio T, Richter H, Weyd M, Wöhner S, Drioli E and Barbieri G 2015 Study of the separation properties of FAU membranes constituted by hierarchically assembled nanozeolites *Sep. Purif. Technol.* **156** 321–7
[12] Itoh N, Ishida J, Kikuchi Y, Sato T and Hasegawa Y 2015 Continuous dehydration of IPA-water mixture by vapor permeation using y type zeolite membrane in a recycling system *Sep. Purif. Technol.* **147** 346–52
[13] Vermeiren W and Gilson J P 2009 Impact of zeolites on the petroleum and petrochemical industry *Top. Catal.* **52** 1131–61
[14] Ng E P and Mintova S 2008 Nanoporous materials with enhanced hydrophilicity and high water sorption capacity *Microporous Mesoporous Mater.* **114** 1–26
[15] Khraisheh M A M, Al-Ghouti M A, Allen S J and Ahmad M N 2005 Effect of OH and silanol groups in the removal of dyes from aqueous solution using diatomite *Water Res.* **39** 922–32
[16] Beta I A, Bohlig H and Hunger B 2004 Structure of adsorption complexes of water in zeolites of different types studied by infrared spectroscopy and inelastic neutron scattering *Phys. Chem. Chem. Phys.* **6** 1975–81
[17] Hunger J, Beta I A, Böhlig H, Ling C, Jobic H and Hunger B 2006 Adsorption structures of water in NaX studied by DRIFT spectroscopy and neutron powder diffraction *J. Phys. Chem. B* **110** 342–53
[18] Kuzniatsova T, Kim Y, Shqau K, Dutta P K and Verweij H 2007 Zeta potential measurements of zeolite Y: Application in homogeneous deposition of particle coatings *Microporous Mesoporous Mater.* **103** 102–7
[19] Ćurković L, Cerjan-Stefanović Š and Filipan T 1997 Metal ion exchange by natural and modified zeolites *Water Res.* **31** 1379–82
[20] Weber W J 1984 Evolution of a technology *J. Snit. Eng. Div.* **110** 899–917
[21] Koltai L, Baksay M and Hungarica S R 2008 Determinations of the colloidal structure of pulp

fibres by adsorption in liquid medium. The role of pulping process *Acta Polytech. Hungarica* **5** 87–92
[22] Chen H, Zhao J, Zhong A and Jin Y 2011 Removal capacity and adsorption mechanism of heat-treated palygorskite clay for methylene blue *Chem. Eng. J.* **174** 143–50
[23] Fungaro D A, Bruno M and Grosche L C 2009 Adsorption and kinetic studies of methylene blue on zeolite synthesized from fly ash *Desalin. Water Treat.* **2** 231–9
[24] Balarak D, Jaafari J, Hassani G, Mahdavi Y, Tyagi I, Agarwal S and Gupta V K 2015 The use of low-cost adsorbent (Canola residues) for the adsorption of methylene blue from aqueous solution: Isotherm, kinetic and thermodynamic studies *Colloids Interface Sci. Commun.* **7** 16–9
[25] Tan I A W, Ahmad A L and Hameed B H 2008 Adsorption of basic dye on high-surface-area activated carbon prepared from coconut husk: Equilibrium, kinetic and thermodynamic studies *J. Hazard. Mater.* **154** 337–46
[26] Shaban M, Abukhadra M R, Shahien M G and Ibrahim S S 2018 Novel bentonite/zeolite-NaP composite efficiently removes methylene blue and Congo red dyes *Environ. Chem. Lett.* **16** 275–80
[27] Sapawe N, Jalil A A, Triwahyono S, Shah M I A, Jusoh R, Salleh N F M, Hameed B H and Karim A H 2013 Cost-effective microwave rapid synthesis of zeolite NaA for removal of methylene blue *Chem. Eng. J.* **229** 388–98
[28] Sohrabnezhad S and Pourahmad A 2010 Comparison absorption of new methylene blue dye in zeolite and nanocrystal zeolite *Desalination* **256** 84–9
[29] Rida K, Bouraoui S and Hadnine S 2013 Adsorption of methylene blue from aqueous solution by kaolin and zeolite *Appl. Clay Sci.* **83**–**84** 99–105
[30] Wang P, Cao M, Wang C, Ao Y, Hou J and Qian J 2014 Kinetics and thermodynamics of adsorption of methylene blue by a magnetic graphene-carbon nanotube composite *Appl. Surf. Sci.* **290** 116–24
[31] Nandi B K, Goswami A and Purkait M K 2009 Removal of cationic dyes from aqueous solutions by kaolin: Kinetic and equilibrium studies *Appl. Clay Sci.* **42** 583–90
[32] Tsai W T, Hsien K J and Hsu H C 2009 Adsorption of organic compounds from aqueous solution onto the synthesized zeolite *J. Hazard. Mater.* **166** 635–41
[33] Miranda L D L, Bellato C R, Fontes M P F, de Almeida M F, Milagres J L and Minim L A 2014 Preparation and evaluation of hydrotalcite-iron oxide magnetic organocomposite intercalated with surfactants for cationic methylene blue dye removal *Chem. Eng. J.* **254** 88–97
[34] Schoonheydt R a. 1992 Clay Adsorbed Dyes: Methylene Blue on Laponite *Clay Miner.* **27** 91–100
[35] Cenens J, Minerals R S-C and C and 1988 U 1988 Visible spectroscopy of methylene blue on hectorite, laponite B, and barasym in aqueous suspension *Clays Clay Miner.* **36** 214–24
[36] Bergmann K and O'Konski C T 1963 A spectroscopic study of methylene blue monomer, dimer, and complexes with montmorillonite *J. Phys. Chem.* **67** 2169–77
[37] Zhang R and Somasundaran P 2006 Advances in adsorption of surfactants and their mixtures at solid/solution interfaces *Adv. Colloid Interface Sci.* **123** 213–29
[38] Qi C, Ge D, Zhu X and Sun Z 2013 Determination of Surface Complexation Constant of Methylene Blue, NH 4+ , Na+ and K+ with SiO2 Surface *Acta Chim. Sin.* **71** 803–9
[39] Li Y, Du Q, Liu T, Peng X, Wang J, Sun J, Wang Y, Wu S, Wang Z, Xia Y and Xia L 2013 Comparative study of methylene blue dye adsorption onto activated carbon, graphene oxide, and carbon nanotubes *Chem. Eng. Res. Des.* **91** 361–8
[40] Wu Z, Zhong H, Yuan X, Wang H, Wang L, Chen X, Zeng G and Wu Y 2014 Adsorptive removal of methylene blue by rhamnolipid-functionalized graphene oxide from wastewater *Water Res.* **67** 330–44